ISSN 2411-3336; e-ISSN 2541-9404

JOURNAL OF MINING INSTITUTE

Zapiski Gornogo instituta

Journal homepage: pmi.spmi.ru

Research article

Geology

Conditions of formation of the Gubanov intrusion of rapakivi granites (Wiborg massif)

Alexey V. Berezin[1], **Ilona V. Rogova**[2]✉, **Sergey G. Skublov**[1,2], **Evgeny I. Grokhotov**[2]

[1] *Institute of Precambrian Geology and Geochronology RAS, Saint Petersburg, Russia*

[2] *Empress Catherine II Saint Petersburg Mining University, Saint Petersburg, Russia*

How to cite this article: Berezin A.V., Rogova I.V., Skublov S.G., Grokhotov E.I. Conditions of formation of the Gubanov intrusion of rapakivi granites (Wiborg massif). Journal of Mining Institute. 2026. Vol. 279. p. 132-151.

Abstract

The article is devoted to determining the *P-T* conditions and formation mechanisms of the Gubanov intrusion (Wiborg rapakivi granite massif) using a suite of petrographic and geochemical methods combined with thermodynamic modelling (rhyolite-MELTS, machine learning). Microstructural analysis of plagioclase resorption made it possible for the first time to estimate the vertical dimension of the intermediate magma chamber at 1.5-2 km and the crystal accumulation/settling timescale (< 0.2 Ma) as the duration of the early stage of rock crystallization. Combined thermobarometry (mineral equilibria, ML algorithms, rhyolite-MELTS) constrained the crystallization interval to T = 840-660 °C, P = 5.5-4.0 kbar at $fO_2 \approx$ FMQ and H_2O in the melt ≈ 6-10 wt.%. It is shown that the rocks of the contact zone between phases formed by partial melting of phase 2 material (producing a melt with 80-84 wt.% SiO_2) triggered by phase 3 melt and subsequent mixing of these components. The results refine the evolutionary model of the Wiborg massif and demonstrate the effectiveness of integrating traditional and modelling petrology methods.

Keywords

rapakivi granites; Wiborg massif; Gubanov intrusion; thermobarometry; fractional crystallization; rhyolite-MELTS; magmatic processes; fluids; post-collisional magmatism

Funding

Petrological modeling was carried out within the framework of the research topic of IPGG RAS “Improvement of isotopic dating methods for Precambrian complexes and development of new geochemical approaches to the use of geochronometer minerals” (FMUW-2022-0005). Fieldwork and sample preparation were supported by the State assignment of Empress Catherine II Saint Petersburg Mining University “Fundamental interdisciplinary studies of the Earth's crust and processes of integrated development of georesources” (FSRW-2023-0002).

Received: 02.07.2025 ***Accepted: 24.12.2025*** ***Online: 26.06.2026*** ***Published: 20.07.2026***

Introduction

Granites are among the most widespread rocks on Earth; their study helps to reveal the processes of continental crust formation [1-3]. Understanding the mechanisms of granite massif formation is critically important [4]. One approach to problems of petrogenesis has been the study of accessory minerals [5, 6], as well as modeling of mineral parageneses [7, 8]. The origin of A-type granites has attracted researchers worldwide for many years. A striking example of this type are rapakivi granites [9]. A wide-ranging association with other rock types complicates determination of their genesis and the geodynamic regime of formation [10, 11]. For a long time rapakivi granites were thought to be usable only as building [12, 13] and facing stone [14, 15]. Discoveries of deposits such as Olympic Dam (Cu-U-Au-Ag-REE), Lac Tio (Fe-Ti-apatite), and others have shown that rock associations including rapakivi granites can be related to a broad range of mineral resources [9].

This is an open access article under the CC BY 4.0 license

Hypotheses on the origin and characteristics of rapakivi granites

Rapakivi granites, characterized by their distinctive texture with ovoids of K-feldspar, represent an important subject for studying magmatic and rock-crystallization processes. Their formation is linked to complex effects of temperature, pressure, and melt composition, yet many aspects of their genesis remain debated. Here we consider two main hypotheses for rapakivi formation.

Magmatic hypotheses propose that rapakivi are formed during the crystallization stage from a melt. K-feldspar ovoids crystallize at temperatures of 750-950 °C, and plagioclase rims form later due to changes in the residual melt composition or a rapid temperature drop [16]. Fluorine plays a key role by increasing the mobility of feldspar components and promoting their redistribution. Experiments show that F-bearing systems exhibit enhanced Na and K diffusion, which facilitates rim formation around ovoids [17]. One variant of rim genesis is their development by subsolidus exsolution of the K-feldspar solid solution during cooling below the solidus (600-700 °C), with plagioclase separating out; fluorine acts as a diffusion catalyst in this process [16]. Some authors suggest crystallization from water-saturated viscous melts, where ovoids form as a result of thixotropic behavior of colloidal systems [17].

Alternative to magmatic hypotheses are models that invoke reworking (including patrial) of sedimentary/metamorphic rocks under high pressures and temperatures, but these models lack sufficient support. In one early hypothesis [18] it was proposed that rapakivi granites formed as a result of metasomatism driven by influx of alkaline fluids that affected Riphean sedimentary and Archean magmatic rocks. A similar point of view was expressed by N.G.Sudovikov [19], who proposed a multi-stage hypothesis. During the first (potassic) stage, K-bearing fluid produced porphyroblasts of K-feldspar in the metamorphic rocks. In the second stage partial melting of the rocks occurred with resorption of the K-feldspar porphyroblasts. In the third and final stage, during decompression, the granite massifs were emplaced to upper crustal levels. Subsequent quantitative studies of the degree of metasomatism, based on a Markov chain statistical model [20], however show that the spatial arrangement of grains in the rock is inconsistent with a model in which rapakivi granites formed by metasomatic generation of large volumes of secondary K-feldspar [19, 21].

Thus, the differences between hypotheses for rapakivi granite formation lie in the dominant processes (magmatic and/or metasomatic), the role of fluids (F, H_2O), and the *P-T* conditions of formation. It is evident that the mechanisms of rapakivi granite formation may be explained by invoking a combination of several hypotheses.

The general sequence of mineral crystallization in rapakivi granites comprises several stages that reflect the evolution of the magmatic system. In early crystallization stages large K-feldspar ovoids form and become crystallization centers. In some cases plagioclase crystallizes earlier, which is related to local variations in melt composition [22]. Plagioclase rims then develop on the ovoids – oligoclase-andesine overgrowing the K-feldspar ovoids. This stage may be associated either with changes in melt composition (an increase in the Ca/Na ratio) or with subsolidus exsolution of the solid solution [21]. Crystallization of the minerals of the groundmass (quartz, biotite, amphibole) occurs in multiple phases, including resorption and recrystallization, indicating dynamic changes in conditions (temperature, fluid regime) [22]. The role of volatiles, especially fluorine, is evident at all stages – it reduces magma viscosity, accelerates diffusion, and stabilizes feldspars, thereby promoting ovoid formation.

Estimates of the formation parameters of rapakivi granites vary considerably depending on the method used. Peak temperatures for intrusive phases associated with injection of hot mantle-derived melts reach 950 °C [23]. Mineral-association analyses, experimental data, and modeling indicate temperatures of 750-780 °C [24]. Pressure during rock formation is estimated at 2-5 kbar (depths of 7-18 km), consistent with near-isothermal decompression during magma ascent. The model implies

This is an open access article under the CC BY 4.0 license

crystallization under conditions of decreasing pressure while temperature remained high [23]. Note that commonly used geothermobarometric methods, such as the Ti-in-zircon thermometer and the Al-in-hornblende barometer, require caution in application – the activity of TiO_2 in zircon depends on pressure and must be calculated correctly, and hornblende compositions may be reequilibrated or fall outside calibration ranges, thereby biasing pressure estimates [23].

Rapakivi granites form in relatively stable tectonic settings, often associated with collisional or post-collisional stages. Their frequent association with anorthosites and mafic rocks indicates a bimodal magmatism in which the granites represent products of interaction between crustal and mantle (mafic) components. It is widely held that rapakivi granites are the result of partial melting of lower-crustal material triggered by thermal input from mantle-derived melts; this is supported by isotopic data (ε_{Nd} from −1 to −4 for Fennoscandian rapakivi) [25, 26]. Modeling of Sr-Nd isotopic system evolution shows mixing of crustal and mantle components, particularly in massifs that contain anorthosites [26].

Although the Wiborg massif is regarded as a typical example of Fennoscandian rapakivi granites, it displays several distinctions from other massifs: predominance of rock varieties with K-feldspar ovoids rimmed by oligoclase [17]; association with gabbro-anorthosite suites indicating a shared magmatic source [26]; high fluorine concentrations (up to 0.5 %) and characteristic rare-earth element patterns in the rocks reflecting melting of lower-crustal granulite sources; crustal isotopic signatures linked to the Paleoproterozoic Fennoscandian crust [26].

A literature review on the topic highlights the following general issues that require further attention:

- Investigation of the conditions of rock formation and correction of inaccuracies in existing estimates caused by limitations of geothermobarometers.
- Assessment of the role of water and the degree of magma water-saturation, since some researchers associate miarolitic cavities with high H_2O content while others link them to fluorine [17].
- The mechanism of ovoid formation remains debated [27]. It is unresolved whether the primary cause is subisothermal decompression or magma mixing. This uncertainty is emphasized by isotopic data that do not always confirm a mantle contribution [23].
- Uncertainty in the geodynamic drivers of lithospheric extension during formation of rapakivi granite massifs – mantle plumes or collisional processes.

In the present study we address only the first and, partially, the second of these questions, with additional examination of the crystallization features of the groundmass, crystallization dynamics, and the genesis of the contact zone between magmatic phases.

Brief geological description

The Wiborg massif is located (Fig.1) in the southeastern part of the Fennoscandian Shield (territory of Finland and Russia) and is the largest pluton of the anorthosite-rapakivi granite formation on the East European Platform. The area of the Wiborg massif exceeds 20,000 km^2 [28, 29]. The Wiborg granite massif is bounded by Proterozoic gneisses and schists whose metamorphic conditions are close to the low-pressure amphibolite facies, although rocks with granulite facies parageneses have also been documented [29, 30]. The contact zone of the massif is represented by augen-bearing quartz diorites and granodiorites, noted along its northern margin [28].

The Wiborg massif was previously studied by D.A.Velikoslavinskii and colleagues [29], A.M.Belyaev [28], O.T.Rämö and I.Haapala [1, 30, 31]; a review of studies is given in the monograph by A.M.Larin [9]. Four magmatic intrusion phases are distinguished within the massif on the Russian territory [28, 29]:

- Phase 1 Lappee granites, represented by pyroxene-hornblende-bearing granites with a minimal quartz content (sienites). Only isolated outcrops of phase 1 have been found in our country [29]. Occurrences of these rocks in the Lappeenranta area have been described in detail by Finnish geologists.

This is an open access article under the CC BY 4.0 license

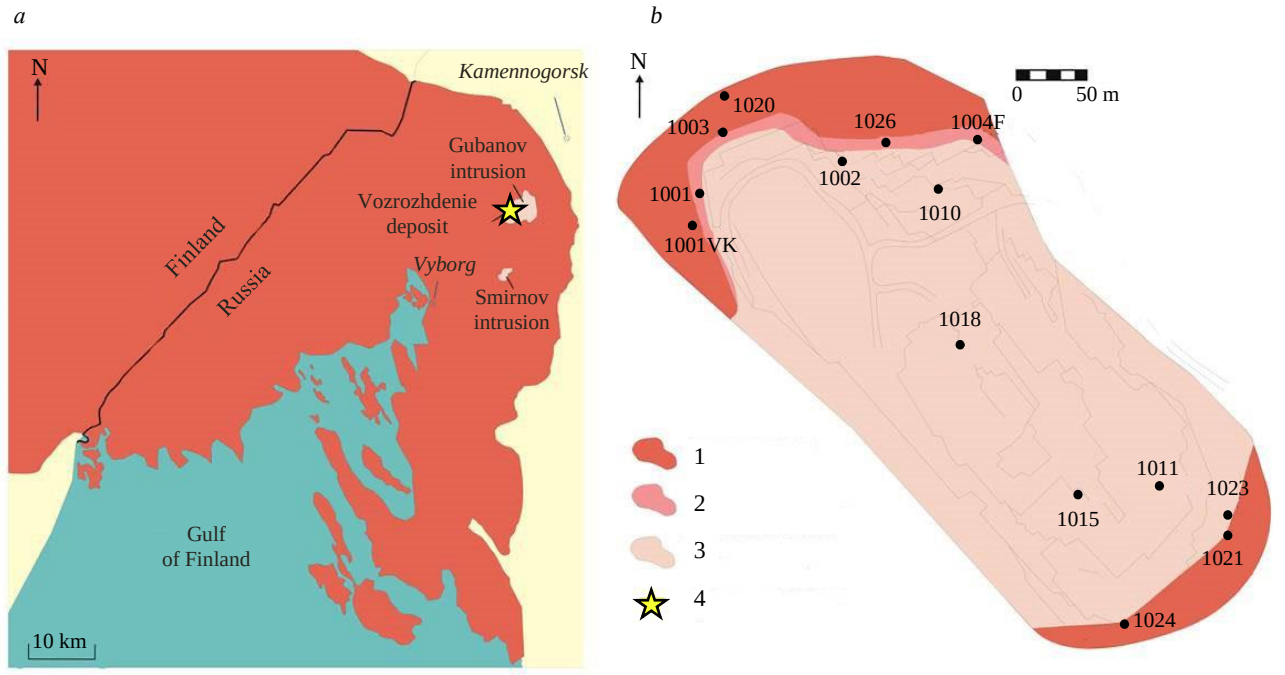


Fig.1. Maps of the eastern part of the Wiborg massif (*a*) and the southwestern part of the Gubanov intrusion exposed by Quarry N 8 of the Vozrozhdenie deposit (*b*)

1 – ovoidal granites (phase 2 granites); 2 – contact zone granites; 3 – trachytoid granites (phase 3 granites); 4 – Vozrozhdenie deposit quarry

• Phase 2 granites are amphibole-biotite ovoidal granites and constitute the greater part of the massif; they are known as Wiborgites.

• Phase 3 trachytoid granites, characteristically pink-gray, have a porphyritic fabric and trachytoid texture. The abundance of ovoids is much lower than in phase 2, about 10-15 %.

• Phase 4 biotite-muscovite topaz-bearing granites have a porphyritic texture with a fine- to medium-grained groundmass [28]. Finnish geologists link the late crystallization stage of the topaz-bearing granites to greisen-type Sn-Be-W-Zn mineralization [30]. Vein bodies such as aplite veins and pegmatites intrude all of the aforementioned rocks, although their inclusion in phase 4 is debatable.

In addition to rapakivi granites, the Wiborg massif contains small bodies of mafic rocks (gabbro-anorthosites, dolerites). These were identified in the Ahvenisto massif; dolerite dikes and, more rarely, quartz porphyries are also found in the Ahvenisto and Suomeniemi areas [28]. Mafic inclusions commonly occur as xenoliths in phase 2 and phase 3 granites.

Because a large part of the Wiborg massif lies within Finland, rock classifications, the number of magmatic phases, and their relationships differ among researchers. Within the Russian territory the greater part of the massif is composed of ovoidal granites (phase 2); two occurrences of phase 3 rapakivi granites (the Gubanov and Smirnov intrusions) have also been described [29]. However, more detailed studies of the rocks were carried out only at discrete localities, and the conclusions drawn remain debated [9, 28, 32]. To study the relationships between phase 2 and phase 3 rapakivi granites of the Wiborg massif, quarry exposures at the Vozrozhdenie building-stone deposit, located northeast of town Vyborg, were selected.

The deposit exposes phase 2 ovoidal granites and phase 3 trachytoid granites (Fig.2). The ovoidal granites outcrop on the northern and southern sides of the quarry, are grey-pink in colour, display an ovoidal fabric (ovoid content ~40-45 %), and have a massive texture. The trachytoid granites are a medium-grained, grey rock with a porphyritic fabric and trachytoid texture (ovoid content < 10 %).

This is an open access article under the CC BY 4.0 license

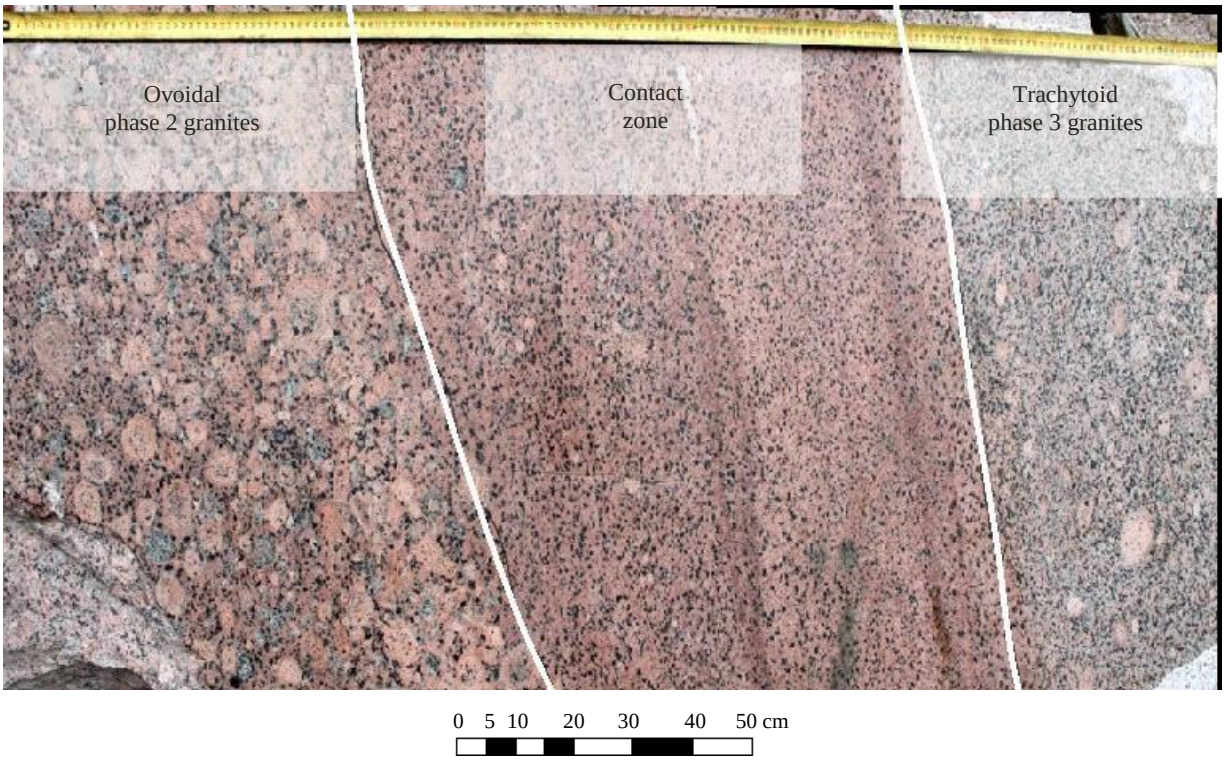


Fig.2. Photograph of the contact zone between phase 2 granites (ovoidal granites) and phase 3 granites (trachytoid granites) in a rock block (unpublished materials used with permission of the Mining Authority "Vozrozhdenie")

The contact zone between the ovoidal and trachytoid granites in the northern part of the quarry varies in thickness from a few centimetres to several metres (Fig.2). It is represented by a fine-grained quartz-feldspar rock of pink colour with biotite "rosettes", which give it a speckled texture. In the southern part of the quarry no exposures of the contact rocks were observed, due to insufficient outcrop and the relatively small thickness of the zone. A detailed description of the mineralogy, petrochemical and geochemical characteristics of the rocks was given by us previously [33].

Methods

Thirty-six samples were collected from the quarry of the Vozrozhdenie deposit. The mineral composition and microstructure of the rocks were studied in optically transparent polished thin-sections of the reference collection (11 thin-sections) on a LEICA DM 750P polarizing microscope (Empress Catherine II Saint Petersburg Mining University). The contents of major elements in the rocks (17 samples) were analyzed by X-ray fluorescence spectrometry (XRF) on a multichannel ARL-9800 spectrometer. The lower detection limits for oxides of major elements are 0.01-0.05 wt.%. Trace and rare-earth elements (REE) in the same samples were measured by inductively-coupled-plasma mass-spectrometry (ICP-MS) on a quadrupole ELAN-DRC-6100 mass-spectrometer (Karpinsky Institute, Saint Petersburg), following preliminary fusion with lithium metaborate and dissolution of the fuse in an acid mixture. Geological USGS standards were used for accuracy control. The relative error for determination of more than 70 elements does not exceed 5-10 %: for REE < 5 %, and for Rb, Sr, Ba, Nb, Ta, Zr, Hf, U, and Th < 10 %. The lower detection limits vary with an accuracy of 0.01 % for major elements and 0.005-0.010 ppm for most REE.

Analysis of photomicrographs of polished thin-sections (calculation of modal mineral proportions and computation of the fractal dimension *D*) was performed using the software ImageJ [34]. Melt viscosity was estimated by two computational methods – a regression approach [35] and the rhyolite-MELTS software package [36]. Note that viscosity calculations were carried out without accounting for fluorine content (up to 0.3 wt.% according to [29]). According to literature data [35, 36],

This is an open access article under the CC BY 4.0 license

such calculations may lead to overestimation of the log η values by 0.1-0.3 un. Thermobarometry of the rocks was performed using several mineral thermometers and barometers.

We applied a machine-learning method (shallow learning – an ensemble random-forest algorithm) to calibrate a regression model that predicts *P-T* conditions of magmas based on the bulk chemical composition of the rock (melt) and the associated mineral assemblage [37]. The model uses an extensive database of experimental data covering compositions from basalt to rhyolite in the pressure range 0.2-15 kbar and temperatures 675-1400 °C. During model training and optimization for internal testing, a filter was applied that removed estimates with a standard deviation above the 50th percentile. This allowed achieving a root-mean-square error (RMSE) for pressure reconstruction of 1.1-1.3 kbar and for temperature of approximately 20 °C.

To estimate the water content in the melt, several methods based on processing experimental data were applied. The first method [38] relies solely on the Na_2O and K_2O contents; the second [39] uses CaO and Al_2O_3 contents and temperature; the third method is represented by the most comprehensive MagmaSat model [40]. This model, integrated with the rhyolite-MELTS [41] software package, accounts for the contents of all rock-forming components as well as temperature, pressure, and the water fraction in the fluid (for granites, H_2O activity is taken as 1). The oxygen fugacity during melt crystallization was evaluated in the rhyolite-MELTS software package [36]. This parameter strongly influences the crystallization sequence and the stability of Fe- and Ti-bearing phases. The convergence criterion was the correspondence between the compositions of modeled mineral phases and those actually observed in the rocks (magnetite and ilmenite).

Crystallization modeling of phases 2 and 3, as well as melting processes during formation of the contact zone, was performed in the rhyolite-MELTS software package (version 1.1.0), which allows a correct assessment of the composition of acidic melts from phase 2. Taking into account petrographic aspects such as plagioclase zoning, the fractional crystallization model was selected for crystallization modeling, while the equilibrium melting model of phase 2 material was used for modeling the formation of the contact zone. Assessment of the composition of theoretical melts from phase 2 granites was carried out by classical methods – using mass-balance equations and subtraction diagrams. Refined numerical estimates were obtained based on regression models [38], constructed from dependencies of melt composition on temperature and pressure (1608 published experimental results), as well as calculations in the rhyolite-MELTS software package, version 1.1.0 [41].

Results and discussion

Mineral composition and textural features of the rocks. Based on petrographic observations, all studied rocks were divided into two groups. The first group includes phase 2 granites, and the second group includes phase 3 granites, as well as contact zone rocks. The mineralogical composition of both groups consists of plagioclase, K-feldspar, quartz, biotite, and amphibole. The main criteria for distinguishing the two rock groups are the tendency toward different compositions of early plagioclase and the nature of its zoning, as well as the intensity of deformation processes during crystallization.

First group (samples 1001, 1106, WGR-23). The rock-forming minerals are represented by plagioclase (An_{15-35}), K-feldspar, quartz, biotite, and, less commonly, amphibole (hornblende). Accessory minerals include zircon and, less commonly, titanite. Plagioclase zoning is less pronounced than in the second group; normal zoning is established. The outer zones of plagioclase grains are more Na-rich (An_{15-25}), whereas the inner zones are more Ca-rich (An_{30-35}), which may indicate formation of the outer zones during cooling.

In the first group, amphibole and biotite show minimal deformation features, and plagioclase zoning is less pronounced, indicating a relatively stable crystallization regime. Amphibole and biotite in the first-group rocks have similar optical orientations and similar extinction characteristics, which may point to their co-crystallization in the magmatic system [42].

This is an open access article under the CC BY 4.0 license

Second group (samples 1010, 1018, 1015, 1026). The rock-forming minerals of the second group consist of plagioclase (An_{22-37}), K-feldspar, quartz, biotite, and, less commonly, amphibole; accessory minerals include zircon, allanite, titanite, and fluorite. Plagioclase displays normal zoning (from An_{37} in cores to An_{22} at grain margins) and signs of resorption. Myrmekite structures are widespread along plagioclase-K-feldspar boundaries; the K-feldspar contains perthites, cryptoperthites, idiomorphic plagioclase inclusions, and also occurs as blocky crystals. Silimanite needles were observed in quartz and K-feldspar. The rocks exhibit deformation microstructures – wavy extinction of quartz and plagioclase, as well as a common optical orientation of amphibole and biotite along deformation zones. The contact zone granites show an elevated quartz content.

The identified features indicate a complex, multi-stage crystallization history accompanied by deformation processes. Normal zoning and resorption of plagioclase, as well as perthitic structures in K-feldspar, reflect fractional crystallization and solid-solution breakdown under changing *P-T* conditions. The presence of blocky K-feldspar crystals likely points to rapid nucleation and growth near the walls of the magmatic chamber [43]. The authors consider the magmatic chamber to be an intermediate chamber. The presence of sillimanite marks relatively high-temperature conditions during the subsolidus stage of crystallization, and the widespread development of myrmekites reflects the relative fluid-saturation of the magmatic system, especially at late magmatic stages of rock evolution. The combination of deformation features (wavy extinction, mineral orientation) confirms the presence of moderate tectonic stresses after the main crystallization stage.

Thus, the rocks of the second group, while showing overall similarity to the first group in mineral composition, are characterized by more intense subsolidus deformation processes and greater mineral compositional variations, which likely relate to their relative position in the final consolidation chamber of the rocks. As noted in [44], textural features such as plagioclase zoning and perthitic structures may be linked to temperature and pressure changes, which is consistent with our conclusions.

Phases 2 and 3 rapakivi granites have similar mineral compositions. Their structural and textural features confirm the conclusion that the magmatic melts crystallized under similar conditions. This fully agrees both with classical petrographic concepts and with geochemical data indicating a common genesis for the ovoidal and trachytoid varieties.

Microstructural evidence for thermal and fluid evolution of the magmatic chamber. Petrographic study of the rocks of the Gubanov intrusion revealed two key microstructural features that carry quantitative information on melt evolution: resorption of zoned plagioclase, recording changes in the thermal regime, and development of myrmekites, marking activation of the fluid phase during late crystallization stages.

Plagioclase resorption as an indicator of vertical movements in the chamber. Plagioclase in the studied rocks (second group) represents one of the earliest phases, and a portion of grains (no more than 5 vol.%) shows resorption features – corroded grain margins and "bay" structures filled with more acidic plagioclase or a quartz-feldspar matrix (Fig.3). Core compositions reach An_{15-37}, whereas outer zones and rims correspond to An_{22-25}. Importantly, resorption is predominantly confined to grain cores and does not affect their outer zones; together with preserved normal zoning, this is characteristic of the magmatic stage.

To estimate the temperature interval of resorption (ΔT), we applied thermodynamic modeling in rhyolite-MELTS. At a fixed pressure of 5 kbar, equilibrium crystallization temperatures for plagioclases with core and rim compositions were calculated. The temperature difference between different zones of plagioclase in resorbed grains reaches up to 80 °C. The observed ΔT range cannot be explained by simple in-situ cooling (other plagioclase grains are not resorbed despite having a similar composition). We interpret this as the result of sinking of early plagioclase crystals into hotter deep parts of the magmatic chamber (or intrusion of a new melt batch). Using the paleogeothermal gradient for 1.6 Ga crust (30-45 °C/km) [45, 46] the depth of this sinking is

This is an open access article under the CC BY 4.0 license

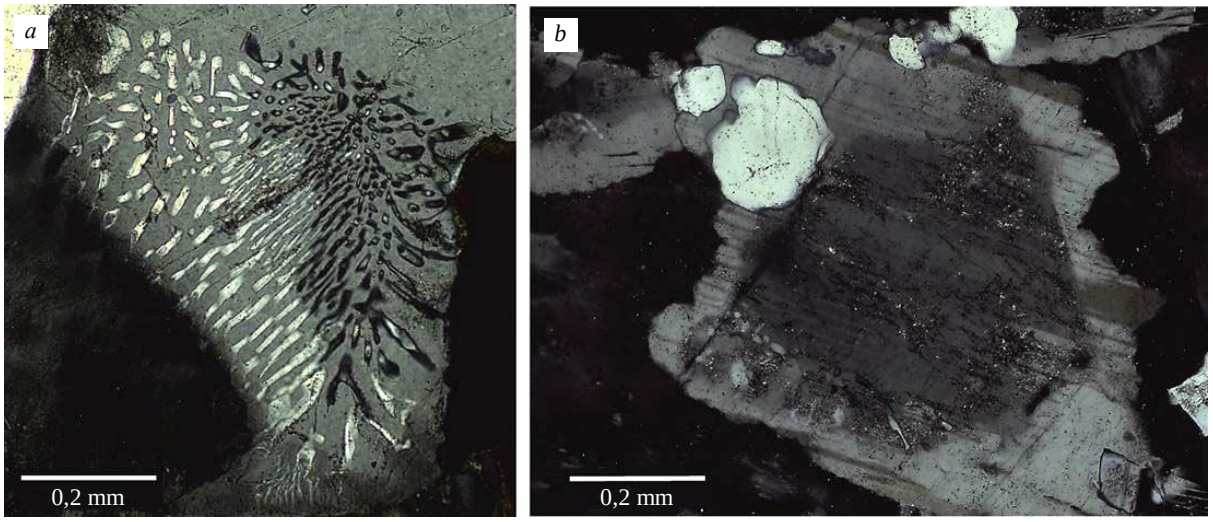


Fig.3. Microscopic photographs (sample 1015, analyzer inserted): *a* – different optical orientations of quartz inclusions in myrmekites; *b* – resorbed plagioclase

estimated by us at 1.5-2 km. Despite the approximate nature of the calculation, this magnitude reflects the possible size of the active magmatic chamber at the time of crystallization of the Gubanov intrusion. Known approximations of the thickness of the earth's crust at the time of crystallization of the rocks of the Gubanov intrusion in the intermediate chamber vary from 50 to 70 km [46, 47], and the value we obtained above fits well with the values corresponding to the thickness of individual intrusions (in this case, the Gubanov intrusion). Note that the inferred magmatic chamber was most likely an intermediate chamber. Alternative hypotheses are also plausible – plagioclase crystallization during decompression or heating by a new magmatic pulse *in situ*.

Using the sizes of resorbed grains, their composition, and calculated estimates of melt viscosity, the sinking time of these crystals in the fluid can be estimated based on Stokes' law. The authors estimated specifically the sinking time of early plagioclase crystals, not the crystallization duration of the entire intrusion. In this calculation, the influence of convective thermal flows in the melt and the change in viscosity in the case of a partially crystallized melt were not considered (coexistence of melt and plagioclase crystals was assumed).

Melt viscosity was estimated by two computational methods – a regression approach [35] and the MELTS software package [36]. For the first method it was 6-7, and for the second – 5 logarithmic units of viscosity (Pa·s), respectively. The melt density estimated in MELTS was 2.34 g/cm^3, and the plagioclase density 2.66 g/cm^3.

Assuming in first approximation that the plagioclase grains are spherical, with maximum and minimum diameters ranging from 0.4 to 0.9 mm, the variations in crystal settling velocity in the silicate fluid are 10^{-12}·10^{-9} m/s. Taking into account the estimated chamber depth of 1.5-2 km, the settling time of plagioclase crystals is at least 0.2 Ma.

The estimated time for complete crystallization of individual phases of the Salmi rapakivi granite massif, made earlier [48], is 3-5 Ma. Our approximate duration for the earliest crystallization stage of the Gubanov intrusion within the Wiborg rapakivi granite massif does not contradict the above estimate.

Myrmekites as indicators of the fluid regime during late stages. The widespread development of myrmekite structures [49] at plagioclase-K-feldspar boundaries (Fig.3) may indicate active interaction of the minerals with a residual fluid-saturated melt. Experimental data by W.Luth and O.Tuttle [50] show that a water fluid in equilibrium with a granitic melt contains dissolved silicate components capable of participating in myrmekite formation. According to N.G.Sudovikov [51], myrmekites can be a product of crystallization of intergranular eutectoid melt enriched in water.

This is an open access article under the CC BY 4.0 license

M.Hibbard [52] links the origin of myrmekites to micro-pressure during the separation of the water phase at late crystallization stages, when plagioclase inclusions grow from the residual melt. A quantitative analysis of myrmekite morphology (fractal dimension assessment) and an estimate of quartz proportion were carried out using quantitative methods in ImageJ software. Recognizing the limitations of two-dimensional sections, we consider the obtained *D* values as a relative indicator of the complexity of quartz inclusion shapes:

- in phase 2 and phase 3 granites, myrmekites are characterized by an elevated quartz proportion (on average 17 vol.%) and a high fractal dimension (*D* up to 1.6), which corresponds to sinuous, "colonial" forms;
- in the contact zone rocks, the quartz proportion in myrmekites decreases to 9 vol.%, and the fractal dimension drops to 1.2-1.3, which correlates with a droplet-like, more equilibrium morphology of the aggregates.

According to published data [53], a high fractal dimension is characteristic of non-equilibrium, skeletal growth forms. Therefore, myrmekites in the main phases formed under conditions of limited diffusion during fluid breakthrough along intergranular boundaries. In contrast, myrmekites in the contact zone with low *D* and droplet-like quartz crystallized under near-equilibrium conditions, presumably at a higher fluid content, which facilitated mass transfer and brought the composition of the residual fluid closer to the pseudoeutectic orthoclase – albite – quartz – water. The estimated An-component content in plagioclase of myrmekites is < 10 mol.% for the contact zone and < 40 mol.% for the main phases [33], which indirectly indicates a lower formation temperature in the former case.

The conducted microstructural analysis allows us to formulate key petrographic constraints for subsequent thermobarometric and thermodynamic reconstructions of genetic models: the vertical chamber size estimate (1.5-2 km), obtained from plagioclase resorption analysis, is a minimum input parameter for pressure variations in crystallization models; the myrmekite morphology indicates that the contact zone between the phases was characterized by elevated fluid saturation. This may support the hypothesis of partial melting of phase 2 material under the influence of the hotter phase 3 melt.

Petrochemical characteristics of the rocks

The petrochemical characteristics of the Gubanov intrusion rocks were given in [33]. We note the main-element compositional features of the rocks that have petrological significance for subsequent modeling. We use several binary variation diagrams that allow us to determine the directions of crystallization trends.

On the SiO_2 – Al_2O_3 diagram, the rock composition points form a trend (Fig.4, *a*); extrapolation of this trend into the high SiO_2 range (hypothetically up to 90-95 wt.%) suggests that the most differentiated residual melts should be enriched solely in silica with Al_2O_3 contents not exceeding 6-7 wt.%. This may indirectly indicate that the most easily melted fraction is represented by SiO_2. The contact zone rocks, which have the highest SiO_2 content, support this assumption. The SiO_2 – Fe_2O_3t diagram shows a similar distribution of rock composition points (Fig.4, *c*). However, continuation of the linear trends into silica-rich compositions suggests that the maximum SiO_2 content in residual melts could reach 80-87 wt.% with extremely low iron contents. Furthermore, on the examined diagrams, extrapolation of the trend to the left side of the composition polygon (the low SiO_2 area) most clearly shows that the assemblages that controlled crystallization at early stages were (Bt + Amp) – (Pl + Fsp) in a 2:3 ratio.

The Al_2O_3 – Fe_2O_3t diagram shows that during fractionation the system became substantially depleted in both aluminum and iron. This is explained by the presence of feldspars and biotite with amphibole (Fig.4, *b*). Considering the diagrams in Fig.4, *b*, *c*, it can be concluded that iron was practically absent in the final crystallization products, although a small amount of aluminum persisted.

This is an open access article under the CC BY 4.0 license

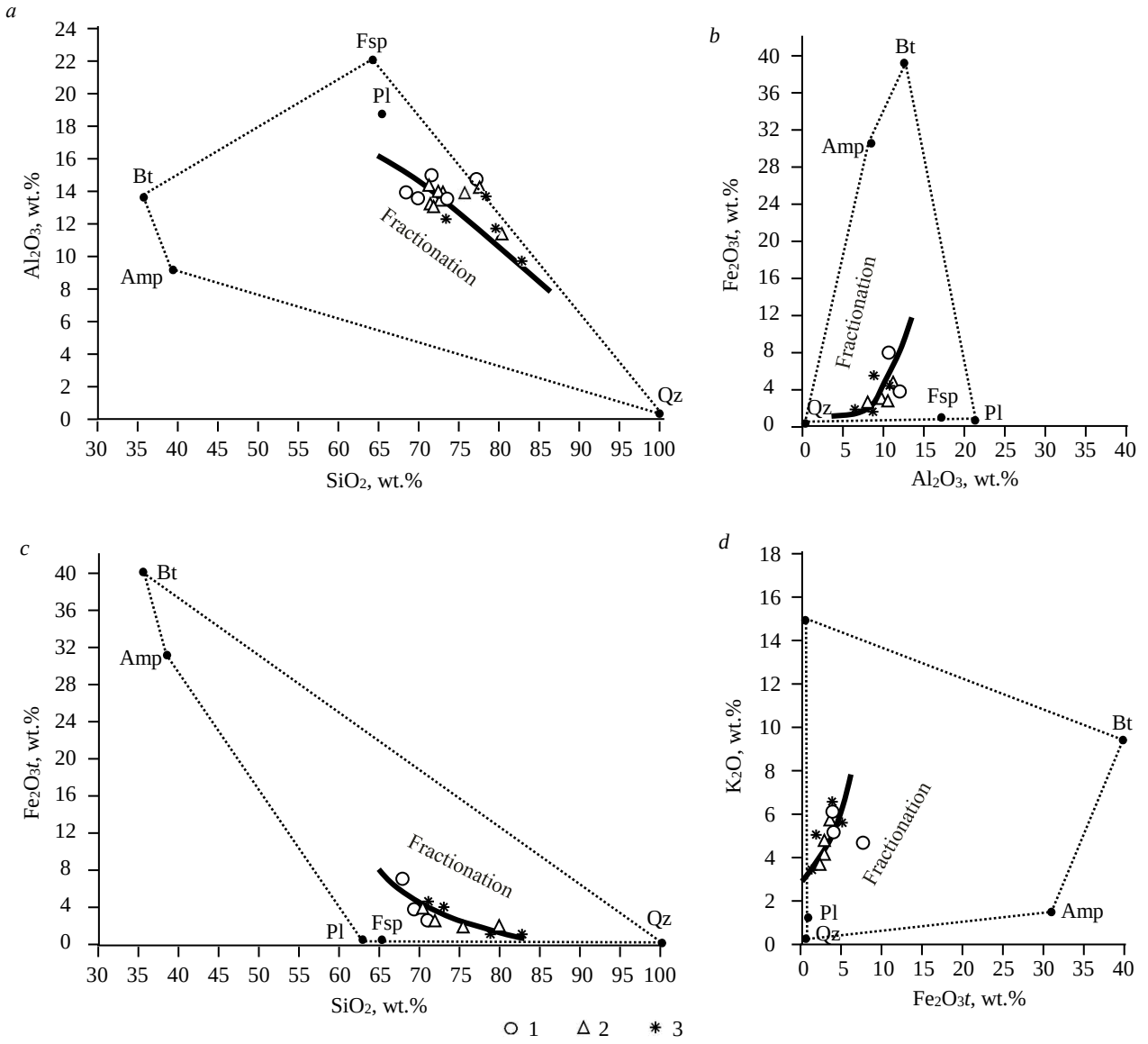


Fig.4. Variation diagrams with evolutionary trends for the granites of the Vozrozhdenie deposit (Wiborg massif), constructed from previously published materials by the authors [33]: *a* – SiO_2 – Al_2O_3; *b* – Al_2O_3 – Fe_2O_3t; c – SiO_2 – Fe_2O_3t; *d* – Fe_2O_3t – K_2O

Magmatic intrusion phases: 1 – phase 2; 2 – phase 3; 3 – contact zone

Using the Fe_2O_3t – K_2O diagram (Fig.4, *d*) and extrapolating the trend into the low Fe_2O_3t range, the K_2O content in the final differentiation products can be estimated at 3-4 wt.%. For the maximum K_2O contents corresponding to orthoclase, Fe_2O_3t in the system should be 16-20 wt.%. This may indicate co-crystallization of orthoclase and iron-rich biotite, or fractionation at early stages with settling of magnetite and ilmenite. Thus, examination of the variation diagrams suggests that phases 2 and 3 granites and the contact zone have a common genetic origin. Early crystallization stages of phase 2 and phase 3 rocks were controlled by fractionation of feldspars and Fe-Mg-phases (biotite and amphibole), whereas the latest differentiated products could be significantly enriched in SiO_2. The SiO_2-most enriched rocks of phase 3 and the contact zone contain virtually no mafic components. Some dispersion of the rock composition points is likely due to the presence of ovoid material.

Consider the Zr – Hf/Eu diagram, which illustrates fractional crystallization processes due to competition between plagioclase fractionation (the main Eu concentrator mineral) and zircon fractionation (determining the Hf/Zr ratio in the rock). Low values of both indicators correspond to the

This is an open access article under the CC BY 4.0 license

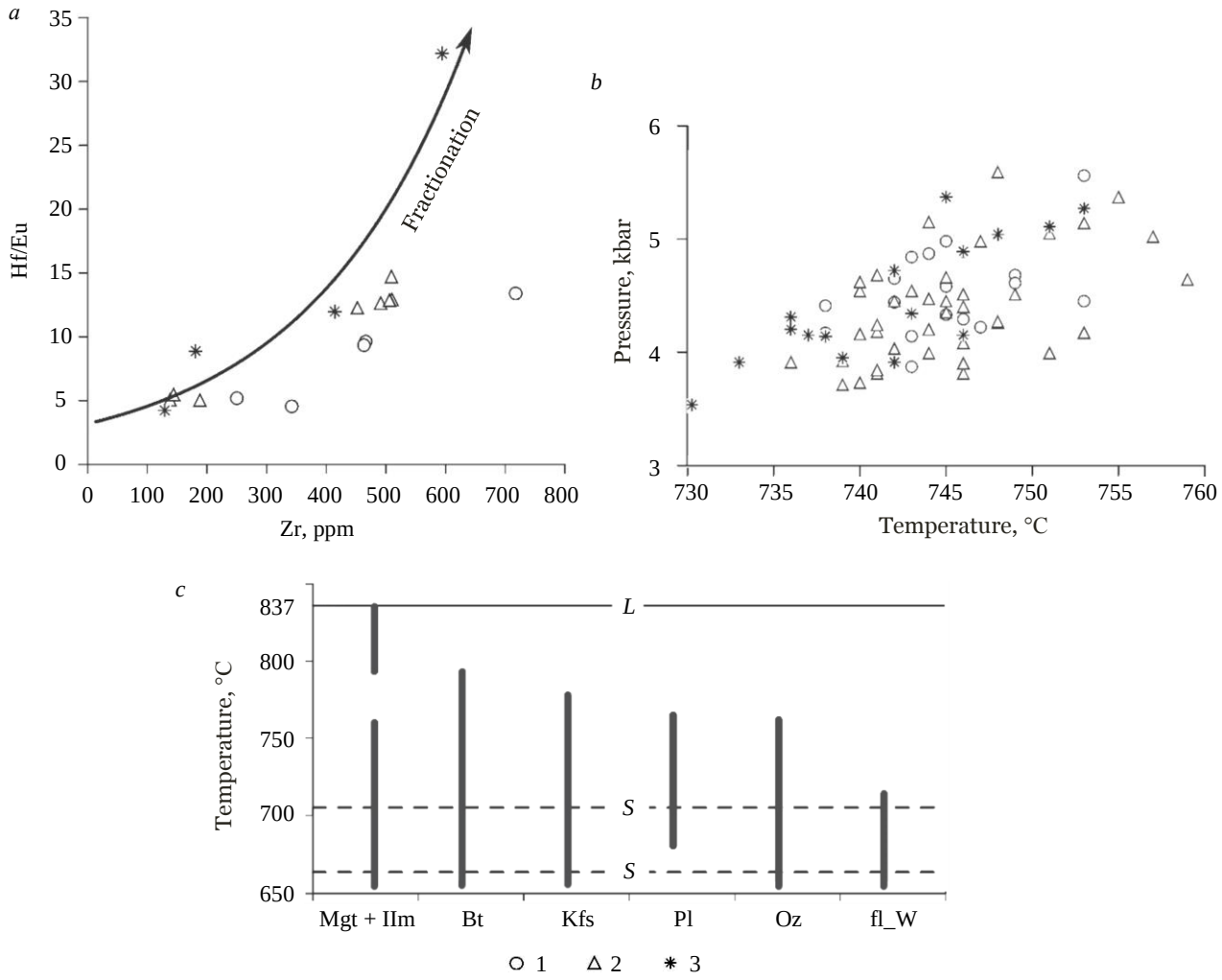


Fig.5. Binary diagram with a rock fractionation trend in Zr – Hf/Eu coordinates (*a*); *P-T* parameters of biotite crystallization in rapakivi granites of phases 2 and 3, as well as in the contact zone between them (*b*); sequence of mineral crystallization based on modeling results for phase 2 and 3 rocks of the Gubanov intrusion (*c*).
Solid line *L* – liquidus temperature; dashed lines *S* – solidus field; mineral abbreviations according to [54]; fl_W – substantially aqueous fluid
Magmatic intrusion phases: 1 – phase 2; 2 – phase 3; 3 – contact zone

least differentiated rocks, and high values to the most differentiated rocks (Fig.5, *a*). Phase 2 and phase 3 rocks have similar Zr contents and an Hf/Eu ratio not exceeding 15. Furthermore, composition points are randomly intermixed on the plot, which may support the hypothesis of a single source for their formation. The contact zone differs markedly from phase 2 and phase 3 rocks, characterized by a minimum Hf/Eu ratio of 3-4, which sharply increases to 30-35 in rocks with zirconium contents of 500-600 ppm (single samples). In contrast, the Hf/Eu ratio in phase 2 and phase 3 rocks is approximately half as large. It should be added that the variations in light rare earth elements are most pronounced precisely in the contact zone rocks, likely due to the elevated zircon content.

These features indicate that the contact-zone rocks are the most differentiated compared with phases 2 and 3 granites. Moreover, phases 2 and 3 granites may be direct components whose mixing and partial melting produce the contact-zone rocks.

Thermobarometry of rocks

Qualitative and mineral thermobarometry. Based on petrographic observations, the range of possible temperatures and pressures of rock formation was estimated from the albite-orthoclase binary diagram for various pressures and the relative proportion of the albite component (5-7 vol.%)

This is an open access article under the CC BY 4.0 license

in orthoclase, according to microprobe data. This approximate estimate allowed us to suggest that the pressure during rock formation was above 3 kbar. The estimated pressure range of 3-5 kbar for rock formation is also confirmed by the presence of allanite and ilmenite in the rock [55]. Using the ternary system albite – orthoclase – quartz ($Ab_{33}Or_{39}Qz_{28}$) as an approximation for granite melt at 3 kbar pressure, the approximate formation temperature of phases 2 and 3 granites was estimated to be no lower than 700 °C [56, 57]. A similar approach can be used to estimate the temperature of myrmekite formation, which is 680-740 °C at pressures from 5 to 2 kbar. Minimum temperatures for the magmatic stage of rock formation can also be estimated based on sillimanite inclusions in quartz and orthoclase. Considering the position of the "average" granite solidus curve relative to the sillimanite stability field, the temperature range for such inclusions was 650-720 °C [58]. Thus, qualitative estimation of mineral parageneses allows constraining the formation parameters of the studied rocks to 800-650 °C by temperature and 5-3 kbar by pressure.

To refine temperatures and pressures, a set of empirical monomineral thermometers and barometers was used. These were applied due to the limited mineral composition and the impossibility of calculating mineral exchange equilibria. All thermometers used were calibrated for the pressure range of interest from 2 to 6 kbar. The resulting temperatures and pressures correspond specifically to the intervals of mineral phase formation, which could crystallize at different degrees of crystallization of the magmatic system. Popular amphibole barometers (based on aluminum content) were not used because our amphibole compositions exceeded the limits of the calibration compositions. However, using the empirical (applicability conditions met – fO_2 = FMQ and presence of ilmenite) thermometer based on titanium content in amphibole [59] (T °C = 2400/(1.52 – log10(Ti_{apfu}) – 273), for contact zone rocks shows a temperature range of 715-815 °C, which is fully consistent with the estimates made above. Using the empirical relationship between Al_2O_3 content in titanite (2.0-4.1 wt.%) and pressure [60] (P = 1.017 Al_2O_3 + 0.59 kbar) a pressure range of 3-5 kbar was obtained, which is close to our estimates based on petrographic data.

The characteristics of the mineral composition do not allow full use of geothermobarometry based on exchange equilibria. One way to address this problem is to use machine learning methods based on experimental data. Using biotite compositions (n = 839, T = 625-1325 °C, P = 1-48 kbar), which covered a wide range (Mg/(Mg + Fe) = 0-1, TiO_2 = 0-9 wt.%), and the so-called random trees/forest method, an empirical biotite thermobarometer was previously calibrated [61]. Error estimation of this model on a test data set shows that root mean square deviations do not exceed 54 °C and 4.4 kbar.

As our calculations for phase 2 and phase 3 granites, as well as for the contact zone, showed, the temperature during biotite crystallization varied in the range of 760-730 °C at pressures from 5.5 to 3.5 kbar. In the *P-T* field, points corresponding to different phases form an elongated area, completely overlapping with each other (Fig.5, *b*). Due to errors comparable to the absolute values of the calculated pressure, these estimates should be considered as very approximate.

To determine pressure, a numerical method for estimating the crystallization of granite intrusions was used, based on two polynomial equations derived from the existing ternary phase diagram of haplogranite and an associated dataset [62],

$$P = -0.0024(Qz)^3 + 0.2639(Qz)^2 - 9.8074(Qz) + 125.63 \text{ kbar};$$

$$P = 0.002426(Ab + Or)^3 - 0.46397(Ab + Or)^2 + 29.813(Ab + Or) - 642.24 \text{ kbar}.$$

The results show that the calculated pressure correlates with the content of normative quartz (Qz), albite (Ab), and orthoclase (Or), with an error of no more than 1.6 kbar. Our calculations indicate that for phase 2 the median pressure is 6.7 kbar, for phase 3 it is 4.9 kbar, and for the contact zone rocks it is 3.9 kbar, respectively. Considering the calculation errors mentioned above, it can be

This is an open access article under the CC BY 4.0 license

assumed that during the crystallization of rock-forming minerals of both intrusion phases and within the contact zone, the pressure was no more than 5 kbar. The noticeable differences in pressure estimates from mineral and polynomial barometers are related to the larger error of the empirical calibration of the latter.

To estimate liquidus temperatures for phase 2 and 3 granites, an empirical method developed for silicate slags was additionally applied [63], which is based on regression analysis of the dependence of liquidus temperature on composition. Although the method is calibrated for dry (anhydrous) systems, we introduced a correction for water content, which reduces the temperature by 50-70 °C. The obtained values (840-880 °C) are in good agreement with estimates from the ML thermobarometer [37] and are close to temperatures calculated in MELTS for dry compositions. However, we consider them as approximate due to the problem of accounting for unanalyzed fluorine content; they could be 5-15 °C lower than calculated.

Estimation of liquidus P-T parameters. The *P-T* parameters estimation using the ML thermobarometer [37] showed that the median temperature is 875 °C for phase 2 granites, 880 °C for phase 3 granites, and 870 °C for contact zone rocks. Considering the method errors, the formation temperatures of the two phases and the contact zone are comparable. The pressure estimates obtained are 6.2 kbar for phase 3; 5.2 kbar for phase 2 and 5.0 kbar for the contact zone. Despite the relatively large scatter of values, these data correlate well with the pressure estimate based on normative quartz content given above – the difference between the two methods is no more than 0.5 kbar.

In general, different methods for estimating *P-T* parameters record different stages of melt evolution, so the temperature scatter is systematic and reflects cooling of the system from liquidus to solidus. Liquidus temperatures (start of crystallization) are no more than 840-880 °C. These estimates refer to early stages when the magma was relatively "dry". Crystallization temperatures of the main mass (biotite, feldspars) are 730-760 °C (from the biotite thermobarometer, Ti-amphibole, and the ternary system Ab – Or – Qz). This corresponds to the 40-60 % crystallization interval of the rocks. Subsolidus temperatures (< 700 °C), determined from myrmekites and the appearance of muscovite/sillimanite in MELTS calculations, correspond to the final stages of rock crystallization. Pressure, estimated by different methods, falls within a relatively narrow range of 6.5-4.2 kbar, averaging about 5 kbar. The obtained estimates practically do not differ from those known for rapakivi granites of the Wiborg massif (760-780 °C and 5-6 kbar), which allows their use in further petrological constructions.

Water content in the melt and oxygen fugacity. In acidic rock types, the content of volatile components, particularly water, plays an important role during crystallization. Calculations for phase 2 and 3 granites ($T \sim 800$ °C, $P \sim 4$ kbar) showed that the maximum possible water concentrations in the melt can reach 9-11 wt.%. In subsequent modeling with the rhyolite-MELTS software package, water content in the melt was set from 6 to 10 wt.%, with 10 wt.% as the upper limit, since the contact zone and late crystallization stages could be water-saturated. Studies [64, 65], based on experimental data, demonstrated that A-type granites can contain the above water amount at 800-900 °C and pressures of 3-7 kbar. It was found that when water content in the melt is below 6 wt.%, the modeled mineral phase compositions differ significantly from those actually observed (e.g., plagioclase compositions become substantially more basic). Similar values were noted previously [54], and the range of possible water contents in the melt varies between 5-11 wt.%. It was established that temperature deviations of up to ±50 °C and pressure deviations of up to 1 kbar in calculations do not affect the calculated H_2O content.

The next parameter to estimate is the oxygen fugacity during melt crystallization. Preliminary modeling (at 5 kbar pressure) for median compositions of phase 2 and 3 granites showed that the

This is an open access article under the CC BY 4.0 license

oxygen fugacity corresponded to the FMQ-FMQ(–1) buffer. The same oxygen fugacity values for rapakivi granite massifs were obtained previously by other researchers [64, 65]. Thus, the conditions for crystallization modeling in the rhyolite-MELTS program are: temperature range 900-500 °C, pressure 5.5-3.5 kbar, and FMQ buffer.

Features of rock crystallization. Let us consider the crystallization features of phase 2 and 3 granites, as well as their contact zone. In a first approximation, this can be done by examining variation diagrams of rock-forming components. Due to the relatively small number of iron-magnesian phases, the system composition can be approximated as oxides of Si, Al, Ca, Na, and K.

Variation diagrams (see Fig.4) were constructed for rock-forming oxides with possible cotectic binary and triple mineral associations. It is quite evident that phase 2 and 3 granites, as well as the contact zone, are genetically related through a common sequence of evolution of the original melt. However, these constructions are more qualitative than quantitative.

Examination of variation diagrams allowed the following hypotheses:

- the most probable early cotectic association was amphibole (and/or biotite) together with plagioclase in a 2:3 ratio;
- the next phase after amphibole was plagioclase with an anorthite component of at least 35 mol.%, confirmed by petrographic and microprobe studies;
- subsequently, the main mass of ovoids crystallized, containing the majority of orthoclase;
- during further crystallization, the main rock mass formed with plagioclase (up to An_{35}) and orthoclase in a 1:1 proportion;
- the late mineral association during crystallization of phase 2 and 3 melts corresponded to a quartz/orthoclase cotectic from 20/80 to 66/33. Note that in the earliest residual melts, these cotectic ratios could reach 75/25 and even higher.

Thus, preliminary data indicate that at late stages of crystallization of phase 2 and 3 melts, and probably also of melts derived from them, the system composition was enriched in silica.

Modeling of phase 2 and 3 crystallization in rhyolite-MELTS showed that mineral appearance temperatures at the liquidus for phases 2 and 3 are similar, so detailed calculations were performed for the median composition of these phases. Adjustment of modeling conditions revealed that real natural mineral associations are best reproduced using a model of fractional polybaric (5.5-3.5 kbar) crystallization with water content in the melt of 6 wt.% or higher. The dP/dT value was 10 bar/°C, consistent with the crustal gradient [45, 46]. For both phases, the liquidus temperature reached 830-840 °C, and the first phase at the liquidus (5.5 kbar) is an Fe-Ti phase – magnetite and ilmenite (Fig.5, *c*). Subsequently, with a slight pressure decrease (to 5 kbar) and at 793 °C, biotite appears (amphibole is also probable), which we identified as inclusions in early K-feldspar and plagioclase. The onset of crystallization of K-feldspar, plagioclase, and quartz occurs practically simultaneously in the 778-762 °C interval at about 4.8 kbar. At this moment, maximum viscosity is recorded ($\log_{10}\eta 5.5$), likely due to fluid enrichment with the quartz component. With further temperature decrease to 714 °C and pressure around 4 kbar, aqueous fluid separation begins, reaching the solidus field at 705-663 °C (4-3.7 kbar). The range of probable solidus temperatures was determined by the sharp drop in melt viscosity logarithm together with its relative fraction. The latest (temperature < 670 °C) subsolidus, and probably metastable, phases are muscovite and sillimanite (identified as inclusions). Overall, it can be concluded that crystallization occurred within a relatively narrow temperature interval of approximately 150-170 °C.

It must be acknowledged that MELTS models provide some idealization of the mineral crystallization order relative to petrographic data: the relatively low iron and magnesium content in our rocks does not allow accurate estimation of the appearance at the liquidus of phases such as biotite

This is an open access article under the CC BY 4.0 license

and amphibole; plagioclase could have started crystallizing before biotite/amphibole if the melt contained less water or more calcium. In our models at 5.5 kbar and 6-10 % H_2O, biotite indeed appears at the liquidus, but with decreasing pressure or water content, plagioclase may become an early phase; the observed "early" plagioclase in the rocks could have undergone sinking and resorption in the lower parts of the chamber under the overall polybaric nature of crystallization. This scenario requires further investigation.

It should be noted that the provided calculations include uncertainties, since the thermodynamic description of biotite does not include its titanium-containing mineral, although in reality biotite is titanium-enriched. The presence of ovoids (up to 6 vol.%) in the rock does not significantly affect the crystallization modeling results for the main rock mass.

Models of contact zone formation. Geological relationships of the phases indicate that phase 2 granites at the time of contact with phase 3 were nearly crystallized but still plastic, since observations (see Fig.2) show that the contact is not sharp and the transition zone has a complex structure. This may indicate interaction between the phases. The preliminary temperature of contact zone formation can probably be estimated as exceeding the rock brittleness temperature (T_{br} = 705-690 °C) by 50-100 °C [63].

Several models for the formation of contact zone rocks can be proposed:

Option A proposes simple mixing of partially crystallized phases 2 and 3 in proportion, according to the mass balance equation,

$$aF2 + (1 - a)F3 = \text{Cont},$$

where a – the proportion of phase 2; Cont, $F2$, and $F3$ – the composition components in the corresponding rocks.

As follows from the chemical compositions of phase 2 and 3 granites (see Supplement, https://pmi.spmi.ru/pmi/article/download/16778/16665), the contact zone differs substantially from them and cannot be a product of their mixing.

Option B proposes nearly complete crystallization of phase 2 granites, followed by thermal impact on them from the heated material of phase 3. Since the temperature of phase 3 material is higher than that of phase 2 granites, the latter begins to melt, and the resulting melt mixes with a more fluid material of phase 3.

This can be described in the form of a mass balance equation

$$aLF2 + (1 - a)F3 = \text{Cont},$$

where $LF2$, $F3$, and Cont are the composition components in the melt and in the rocks, respectively.

Features of this model: The composition of the melt formed from phase 2 should be close to eutectic; the temperature of phase 3 does not necessarily need to correspond to the maximum (liquidus) temperature, since the system was partially crystallized. Other mixing variants exist: the melt mixes simultaneously with both the partially crystallized material of phase 2 and the melt of phase 3; the residual melt of phase 3 mixes with the partially crystallized material of phase 2. Given the similarity of compositions of possible mixing participants, we chose the simplest model variant (Option B). At viscosity logη 5 (water-saturated phase 3 melt), limited interaction with the nearly crystallized but heated phase 2 is quite probable. This is not mechanical mixing of two liquids, but rather infiltration of residual melt with local component redistribution. The absence of macroscopic signs of partial melting in phase 2 does not contradict the proposed model. Experimental studies show that at 700-800 °C temperatures and with aqueous fluid present, the first melt from granitoids has a eutectic/subeutectic composition and extremely low viscosity [50, 52]. Under such conditions, even small melt volumes (< 5 vol.%) can be efficiently extracted from the parent substrate by infiltration along intergranular boundaries, without leaving large corrosion structures [66]. Our calculated melt proportion (~2 % of the volume of phase 2) agrees with the absence of visible structural-textural signs of melting and confirms the proposed residual melt infiltration mechanism.

This is an open access article under the CC BY 4.0 license

Estimation of melt composition. Several methods exist to estimate the melt that, when mixed with phase 3 material, yields the contact zone composition.

The first method is based on an inverse calculation using the mass-balance equation in Option B. By fixing the contact-zone composition and phase 3 composition (see Supplement, https://pmi.spmi.ru/pmi/article/download/16778/16665), one can select a melt composition and its proportion such that the component contents in the melt are non-negative. This estimate shows that the melt proportion in the mixture must be at least 0.5 wt.%, and its SiO_2 content approximately 80 wt.%.

The second method uses subtraction diagrams. This method is approximate, considering only the mass-balance equation, and does not account for the thermodynamics of the crystallization process and reaction relationships. As seen in Fig.4, for phases 2 and 3 the composition points form an elongated area that can be approximated by linear trends. This primarily indicates that during phase crystallization, the mineral proportion in the cotectic association changed little. Accordingly, by extrapolating points toward the low-silica region, we should intersect the polygon of compositions of phases that controlled crystallization. Similarly, by extending the line toward maximum compositions, we obtain an estimate of the residual melt, the most easily meltable. Obviously, all rock compositions, as well as the original melt, must lie between the composition points of the initial cotectic association and the residual melt. Variation diagrams were constructed for all possible oxide combinations, and a linear trend was drawn for each. The position of the point (on the trend extension) of the assumed melt was selected so that there were no negative contents and the sum of all components equal 100 wt.%. After examining all possible oxide combinations, the assumed melt composition was obtained with an SiO_2 content of approximately 84 wt.%. An approximate calculation showed that the melt proportion must be at least 0.32 wt.%.

The third method, based on regression relationships between melt chemical composition and temperature and pressure [38], showed that the melt proportion must be at least 0.39 wt.%, and the SiO_2 content in the melt approximately 81 wt.%.

The fourth method applied an equilibrium melting model of phase 2 in rhyolite-MELTS [41], which indicated that at least 69 % melt in the mixture (+31 % phase 3 material) is required to obtain the contact zone composition. Note that the relative amount of melt from phase 2 probably did not exceed 2 % (the amount of melt actually extracted from phase 2 relative to the entire mass of this phase), which overall agrees with the small thickness of the contact zone.

Modeling was performed for sequential batch melting (analogous to fractional crystallization). However, this variant showed poorer convergence compared to the equilibrium variant. The minimum melt proportion for contact-zone formation was 40 % in both the equilibrium and fractional melting cases, and the SiO_2 content in the melt was 73-75 wt.%. More complex melting models, including those involving incomplete melting of ovoid material, also cannot be excluded.

Comparing the four methods for calculating the contact-zone composition relative to the real one (Fig.6, see Supplement, https://pmi.spmi.ru/pmi/article/download/16778/16665), it can be concluded that all calculation methods yield comparable results, with uncertainties not exceeding 2 wt.% (2σ); the minimum melt proportion required to obtain the contact-zone composition in mixture with phase 3 varies from 0.32 to 0.69 wt.%; the method with the smallest relative errors is the variation-diagram method. If the melting degree of phase 2 was low (~0.02) while its proportion in the mixture with phase 3 was high (~0.69), this means that the melt from phase 2 intensively mixed with a large volume of phase 3 melt.

Thus, a model for the formation of the contact zone (Fig.7) can be presented, which most likely corresponds to its formation mechanism, and the observed compositions of contact-zone granites agree satisfactorily with the model.

This is an open access article under the CC BY 4.0 license

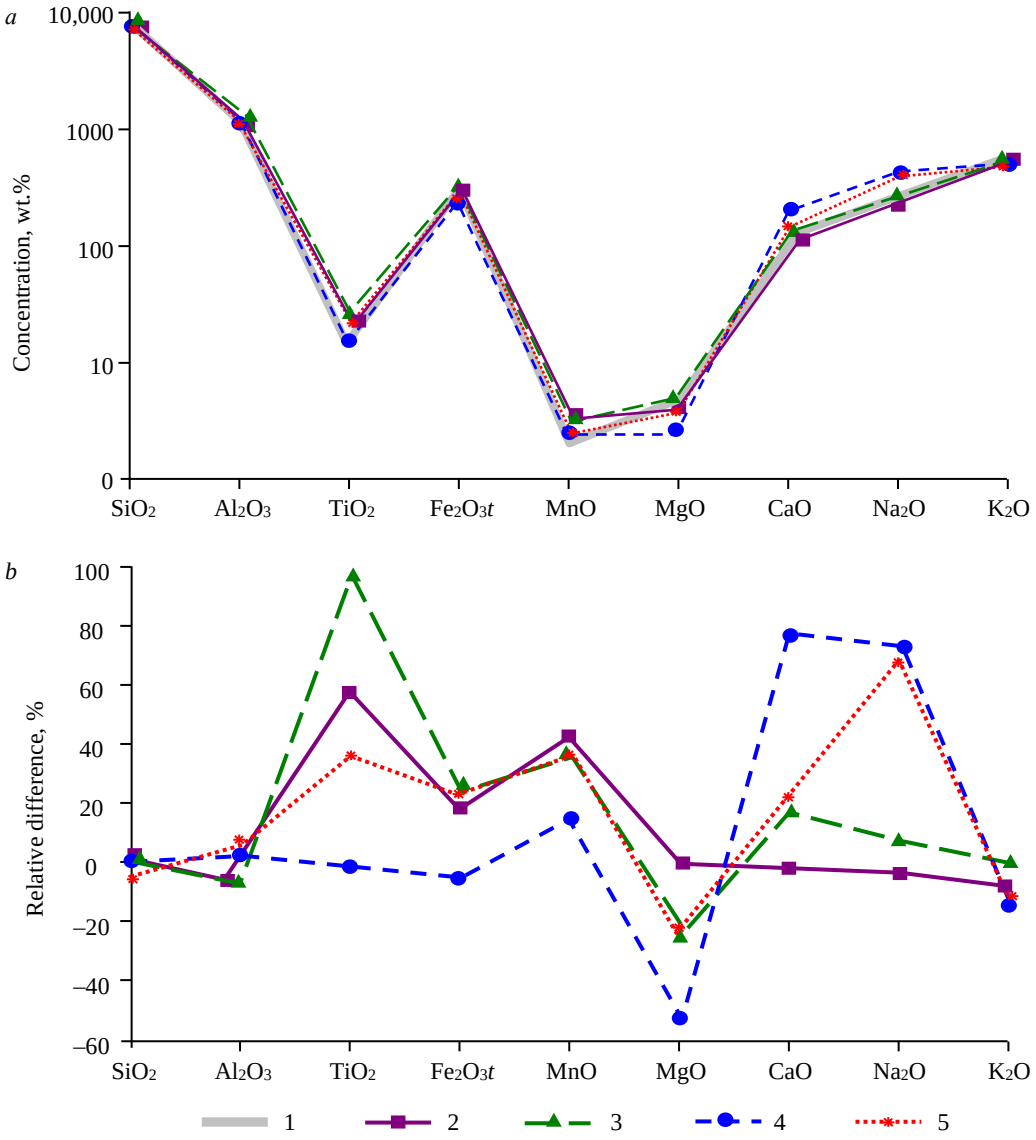


Fig.6. Comparative graphs of contact zone modeling results (*a*); differences between model and real contact zone compositions for various formation models (*b*)

1 – contact zone composition; 2 – variation diagrams; 3 – mass-balance calculation; 4, 5 – MELTS melting modeling (version 1.1.0): equilibrium (4), fractional (5)

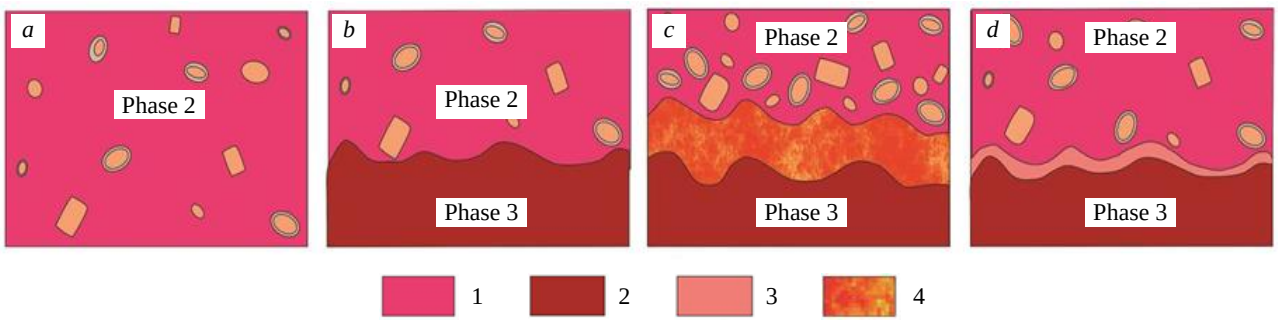


Fig.7. Model of contact zone formation: *a* – stage of partial crystallization of phase 2 granites; *b* – heating of phase 2 granites during phase 3 intrusion; *c* – formation of partial melt from phase 2; *d* – mixing of uncrystallized melt from phase 2 and partially crystallized material of phase 3

1 – phase 2 melt; 2 – phase 3 melt; 3 – melt from phase 2; 4 – contact zone

This is an open access article under the CC BY 4.0 license

Conclusion

The comprehensive study of the Gubanov intrusion yielded the following new quantitative constraints for the petrogenetic model of rapakivi granites of the Wiborg massif:

- Combining machine learning methods, thermodynamic modeling, and experimentally calibrated mineral thermometers, with strict applicability criteria, allowed highly reliable reconstruction of the crystallization evolution of the Gubanov intrusion. Liquidus temperatures determined by the ML method and rhyolite-MELTS are 880-840 °C. Crystallization of the main rock volume occurred at 790-760 °C and began with biotite and/or amphibole crystallization. Final crystallization and subsolidus processes, marked by the sillimanite paragenesis, occurred at 720-650 °C. Pressure, reliably determined from the convergence of ML modeling results and normative phase compositions, systematically decreased from 5.5 to 4.0 kbar, consistent with polybaric melt evolution with significant water influence (up to 6-10 wt.%) and oxygen fugacity at the FMQ buffer level affecting the phase crystallization order.
- For the first time, for intrusions of this type, based on analysis of plagioclase resorption, the vertical size of the active intermediate chamber was quantitatively estimated (at least 1.5-2 km), and it was shown that early crystals could undergo gravitational settling/migration over ~0.2 Ma. Myrmekite morphometric analysis confirmed high fluid saturation of the system at the final crystallization stages, especially in the phase contact zone.
- Modeling in rhyolite-MELTS and mass-balance calculations refuted the hypothesis of simple mixing of phase 2 and 3 magmas. A model was substantiated, according to which contact zone rocks are a product of mixing high-silica melt (SiO_2 ~80-84 wt.%), formed by partial melting of nearly crystallized phase 2 under the thermal impact of phase 3 melt, together with the phase 3 melt itself.
- It was shown that combining classical petrography, geochemistry, thermodynamic modeling, and machine learning methods minimizes errors and uncertainties inherent to each method individually and provides the most complete picture of the evolution of complex magmatic systems.

The results support the formation of the Gubanov intrusion in a post-collisional extension setting, where fractional crystallization and local thermal interaction between sequential intrusion phases played the leading role.

Access to data

Supplement is available at the link: https://pmi.spmi.ru/pmi/article/download/16778/16665.

The authors thank E.N.Kuzminykh and K.S.Gusak (*Mining Authority* "*Vozrozhdenie*") *for organizing field works.*

REFERENCES

1. Rämö O.T., Haapala I. One hundred years of rapakivi granite. *Mineralogy and Petrology*. 1995. Vol. 52. Iss. 3-4, p. 129-185. DOI: 10.1007/BF01163243

2. Yakymchuk C. On Granites. *Journal of the Geological Society of India*. 2019. Vol. 94. N 1, p. 9-22. DOI: 10.1007/s12594-019-1261-2

3. Shatov V.V., Tkachenko M.A., Zubova T.N. et al. Revealing the porphyry copper-gold potential in granitoid complexes of the Russian Federation based on Porphyry Indicator Zircons (PIZs). *Regional Geology and Metallogeny*. 2024. Vol. 31. N 4 (100), p. 126-146 (in Russian). DOI: 10.52349/0869-7892_2024_100_126-146

4. Alekseev V.I., Marin Yu.B. On the Genesis of "White Granite" from the Kester Harpolith, Arga-Ynnakh-Khaya Pluton, East Yakutia. *Geology of Ore Deposits.* 2020. Vol. 62. N 8, p. 719-730. DOI: 10.1134/S1075701520080024

5. Alekseev V.I., Marin Yu.B. Accessory Cassiterite as an Indicator of Rare Metal Petrogenesis and Mineralization. *Geology of Ore Deposits.* 2022. Vol. 64. N 7, p. 397-423. DOI: 10.1134/S1075701522070029

6. Alekseev V.I., Marin Yu.B., Galankina O.L. Wolframoixiolite in Lithium-Fluorine Granites of the Arga-Ynnakh-Khaya Pluton, Yakutia. *Geology of Ore Deposits.* 2020. Vol. 62. N 7, p. 629-637. DOI: 10.1134/S1075701520070028

This is an open access article under the CC BY 4.0 license

7. Marin Yu.B., Smolensky V.V., Beskin S.M. Geological Position, Features of Mineralization and Typifcation of Rare-Metal – Rare-Earth Amazonite Pegmatites. *Zapiski Rossiiskogo mineralogicheskogo obshchestva.* 2025. Vol. 154. N 2, p. 3-13 (in Russian). DOI: 10.31857/S0869605525020018

8. Gulbin Yu.L., Mikhalsky E.V. Modeling of Mineral Parageneses and Thermobarometry of Metavolcanic Rocks of the Ruker Group in the Southern Prince Charles Mountains, East Antarctica. *Geology of Ore Deposits.* 2020. Vol. 62. N 7, p. 584-598. DOI: 10.1134/S1075701520070053

9. Larin A.M. Rapakivi Granites and Associated Rock. St. Petersburg: Nauka, 2011, p. 402 (in Russian).

10. Vladimirov A.G., Izokh A.E., Polyakov G.V. et al. Gabbro-Granite Intrusive Series and Their Indicator Importance for Geodynamic Reconstructions. *Petrology.* 2013. Vol. 21. N 2, p. 158-180. DOI: 10.1134/S0869591113020070

11. Jingya Cao, Xiaoyong Yang, Jianguo Du et al. Formation and geodynamic implication of the Early Yanshanian granites associated with W-Sn mineralization in the Nanling range, South China: an overview. *International Geology Review*. 2018. Vol. 60. Iss. 11-14, p. 1744-1771. DOI: 10.1080/00206814.2018.1466370

12. Bulakh A.G., Popov G.N., Yanson S.Yu., Ivanov M.A. New data on the granite pedestal of the monument to Peter the Great "The Bronze Horseman" in Saint Petersburg. *Journal of Mining Institute.* 2021. Vol. 248, p. 180-189. DOI: 10.31897/PMI.2021.2.2

13. Daniliev S.M., Danilieva N.A., Isakova E.P., Ashkar G.K. Research of cracking at facing stone deposit using the georadar method. *Bulletin of the Tomsk Polytechnic University. Geo Assets Engineering.* 2020. Vol. 331. N 9, p. 140-145 (in Russian). DOI: 10.18799/24131830/2020/9/2816

14. Ivanov M.A. Mineralogical characteristics and spatial distribution of different age fractures in granites and pegmatites of the "Vozrozhdenie" deposit ("Kawantsaari"), the Vyborg massif. *Journal of Mining Institute.* 2015. Vol. 212, p. 21-29 (in Russian).

15. Kameneva E.E., Nikiforova V.S. Study of the pore structure in granite and gabbrodolerite crushed stone grains of various sizes. *Journal of Mining Institute.* 2025. Vol. 271, p. 74-83.

16. Dempster T.J., Jenkin G.R.T., Rogers G. The Origin of Rapakivi Texture. *Journal of Petrology*. 1994. Vol. 35. Iss. 4, p. 963-981. DOI: 10.1093/petrology/35.4.963

17. Elliston J.N. Rapakivi texture: An indication of the crystallization of hydrosilicates, II. *Earth-Science Reviews*. 1985. Vol. 22. Iss. 1, p. 1-92. DOI: 10.1016/0012-8252(85)90039-X

18. Backlund H.G. The problems of the rapakivi granites. *The Journal of Geology*. 1938. Vol. 46. N 38. Part 2, p. 339-396.

19. Sudovikov N.G. Problem of rapakivi and late orogenic intrusions. Leningrad: Nauka, 1967, p. 118 (in Russian).

20. Podkovyrov V.N. Origin of rapakivi granites by stochastic modeling: Vyborg and Salmi Massifs. *Mathematical Geology*. 1987. Vol. 19. Iss. 7, p. 697-717. DOI: 10.1007/BF00897575

21. Levkovskii R.Z. Rapakivi. Leningrad: Nedra, 1975, p. 223 (in Russian).

22. Emslie R.F. Granitoids of rapakivi granite-anorthosite and related associations. *Precambrian Research*. 1991. Vol. 51. Iss. 1-4, p. 173-192. DOI: 10.1016/0301-9268(91)90100-O

23. Heinonen A.P., Rämö O.T., Mänttäri I. et al. Zircon as a Proxy for the Magmatic Evolution of Proterozoic Ferroan Granites; the Vyborg Rapakivi Granite Batholith, SE Finland. *Journal of Petrology*. 2017. Vol. 58. Iss. 12, p. 2493-2517. DOI: 10.1093/petrology/egy014

24. Eklund O., Shebanov A.D. The origin of rapakivi texture by sub-isothermal decompression. *Precambrian Research*. 1999. Vol. 95. Iss. 1-2, p. 129-146. DOI: 10.1016/S0301-9268(98)00130-2

25. Dall'Agnol R., Teixeira N.P., Rämö O.T. et al. Petrogenesis of the Paleoproterozoic rapakivi A-type granites of the Archean Carajás metallogenic province, Brazil. *Lithos*. 2005. Vol. 80. Iss. 1-4, p. 101-129. DOI: 10.1016/j.lithos.2004.03.058

26. Heinonen A.P., Andersen T., Rämö O.T. Re-evaluation of Rapakivi Petrogenesis: Source Constraints from the Hf Isotope Composition of Zircon in the Rapakivi Granites and Associated Mafic Rocks of Southern Finland. *Journal of Petrology*. 2010. Vol. 51. Iss. 8, p. 1687-1709. DOI: 10.1093/petrology/egq035

27. Vernon R.H. A Practical Guide to Rock Microstructure. Cambridge University Press, 2018, p. 442.

28. Belyaev A.M. Mineralogical and Geochemical Specialization of the Rapakivi Granites of the Vyborg Massif. *Vestnik LGU*. 1983. Vol. 6. N 1, p. 17-26 (in Russian).

29. Velikoslavinskii D.A., Birkis A.P., Bogatikov O.A. et al. Anorthosite-rapakivigranite formation of the East European Platform. Leningrad: Nauka, 1978, p. 296 (in Russian).

30. Haapala I. Metallogeny of the rapakivi granites. *Mineralogy and Petrology*. 1995. Vol. 54, p. 149-160.

31. Haapala I., Rämö O.T., Frindt S. Comparison of Proterozoic and Phanerozoic rift-related basaltic-granitic magmatism. *Lithos*. 2005. Vol. 80. Iss. 1-4, p. 1-32. DOI: 10.1016/j.lithos.2004.04.057

32. Sviridenko L.P. Petrology of rapakivi granites in Salmi massif. Petrozavodsk: Karelskoe knizhnoe izdatelstvo, 1968, p. 116 (in Russian).

33. Rogova I.V., Skublov S.G., Berezin A.V., Petrov D.A. Geochemical characterization of Gubanovskaya intrusion of rapakivi granites (Wiborg massif). *Vestnik of MSTU.* 2025. Vol. 28. N 1, p. 26-37 (in Russian). DOI: 10.21443/1560-9278-2025-28-1-26-37

34. Collins T.J. ImageJ for microscopy. *BioTechniques*. 2007. Vol. 43. Iss. 1 (Suppl.), p. S25-S30. DOI: 10.2144/000112517

35. Baker D.R. Granitic melt viscosities: Empirical and configurational entropy models for their calculation. *American Mineralogist*. 1996. Vol. 81. N 1-2, p. 126-134. DOI: 10.2138/am-1996-1-216

36. Gualda G.A.R., Ghiorso M.S., Lemons R.V., Carley T.L. Rhyolite-MELTS: a Modified Calibration of MELTS Optimized for Silica-rich, Fluid-bearing Magmatic Systems. *Journal of Petrology*. 2012. Vol. 53. Iss. 5, p. 875-890. DOI: 10.1093/petrology/egr080

37. Weber G., Blundy J. A Machine Learning-Based Thermobarometer for Magmatic Liquids. *Journal of Petrology*. 2024. Vol. 65. Iss. 4. N egae020. DOI: 10.1093/petrology/egae020

38. Winther K.T. A model for estimating the composition of partial melts. *Mineralogy and Petrology*. 1995. Vol. 53. Iss 1-3, p. 189-195. DOI: 10.1007/BF01171956

39. Gnuchev Ya.Yu., Bychkov D.A., Koptev-Dvornikov E.V. An Equation for the Calculation of Saturated Water Contents in Silicate Melts: A New Version. *Geochemistry International.* 2023. Vol. 61. N 9, p. 937-947. DOI: 10.1134/S0016702923090045

This is an open access article under the CC BY 4.0 license

40. Iacovino K., Matthews S., Wieser P.E. et al. VESIcal Part I: An Open-Source Thermodynamic Model Engine for Mixed Volatile (H_2O-CO_2) Solubility in Silicate Melts. *Earth and Space Science*. 2021. Vol. 8. Iss. 11. N e2020EA001584. DOI: 10.1029/2020EA001584

41. Ghiorso M.S., Gualda G.A.R. An H_2O-CO_2 mixed fluid saturation model compatible with rhyolite-MELTS. *Contributions to Mineralogy and Petrology*. 2015. Vol. 169. Iss. 6. N 53. DOI: 10.1007/s00410-015-1141-8

42. Fiedrich A.M., Bachmann O., Ulmer P. et al. Mineralogical, geochemical, and textural indicators of crystal accumulation in the Adamello Batholith (Northern Italy). *American Mineralogist*. 2017. Vol. 102. N 12, p. 2467-2483. DOI: 10.2138/am-2017-6026

43. Vernon R.H. K-feldspar megacrysts in granites – Phenocrysts, not porphyroblasts. *Earth-Science Reviews*. 1986. Vol. 23. Iss. 1, p. 1-63. DOI: 10.1016/0012-8252(86)90003-6

44. Vernon R.H. Rapakivi granite problems: plagioclase mantles and ovoid megacrysts. *Australian Journal of Earth Sciences*. 2016. Vol. 63. Iss. 6, p. 675-700. DOI: 10.1080/08120099.2016.1241953

45. Weihed P., Arndt N., Billström K. et al. Precambrian geodynamics and ore formation: The Fennoscandian Shield. *Ore Geology Reviews*. 2005. Vol. 27. Iss. 1-4, p. 273-322. DOI: 10.1016/j.oregeorev.2005.07.008

46. Kukkonen I.T., Lauri L.S. Modelling the thermal evolution of a collisional Precambrian orogen: High heat production migmatitic granites of southern Finland. *Precambrian Research*. 2009. Vol. 168. Iss. 3-4, p. 233-246. DOI: 10.1016/j.precamres.2008.10.004

47. Puura V., Flodén T. Rapakivi-granite-anorthosite magmatism – a way of thinning and stabilisation of the Svecofennian crust, Baltic Sea Basin. *Tectonophysics*. 1999. Vol. 305. Iss. 1-3, p. 75-92. DOI: 10.1016/S0040-1951(99)00019-0

48. Amelin Y.V., Larin A.M., Tucker R.D. Chronology of multiphase emplacement of the Salmi rapakivi granite-anorthosite complex, Baltic Shield: implications for magmatic evolution. *Contributions to Mineralogy and Petrology*. 1997. Vol. 127. Iss. 4, p. 353-368. DOI: 10.1007/s004100050285

49. Jiashu Rong, Fenggang Wang. Metasomatic Textures in Granites. Springer, 2025, p. 172. DOI: 10.1007/978-981-97-1590-9

50. Luth W.C., Tuttle O.F. The Hydrous Vapor Phase in Equilibrium with Granite and Granite Magmas. *Igneous and Metamorphic Geology*. Geological Society of America, 1969. DOI: 10.1130/MEM115-p513

51. Sudovikov N.G. Tectonics, metamorphism, migmatization, and granitization of the Ladoga formation rocks. Moscow; Leningrad: Izd-vo Akademii nauk SSSR, 1954, p. 199 (in Russian).

52. Hibbard M.J. Myrmekite as a marker between preaqueous and postaqueous phase saturation in granitic systems. *GSA Bulletin*. 1979. Vol. 90. N 11, p. 1047-1062. DOI: 10.1130/0016-7606(1979)90<1047:MAAMBP>2.0.CO;2

53. Fowler A.D. Self-organized mineral textures of igneous rocks: the fractal approach. *Earth-Science Reviews*. 1990. Vol. 29. Iss. 1-4, p. 47-55. DOI: 10.1016/0012-8252(0)90027-S

54. Guo-Neng Chen, Grapes R. Granite Genesis: In-Situ Melting and Crustal Evolution. Springer, 2007. DOI: 10.1007/978-1-4020-5891-2

55. Li Xiao-Wei, Huang Xiong-Fei, Huang Dan-Feng. Review on Application of Geobarometry for Granitic Rocks. *Geological Journal of China Universities*. 2011. Vol. 17. N 3, p. 415-422 (in Chinese).

56. Pichavant M., Holtz F., McMillan P.F. Phase relations and compositional dependence of H_2O solubility in quartz-feldspar melts. *Chemical Geology*. 1992. Vol. 96. Iss. 3-4, p. 303-319. DOI: 10.1016/0009-2541(92)90061-9

57. Pichavant M., Weber C., Villaros A. Effect of anorthite on granite phase relations: Experimental data and models. *Comptes Rendus Géoscience*. 2019. Vol. 351. N 8, p. 540-550. DOI: 10.1016/j.crte.2019.10.001

58. Joyce D.B., Voigt D.E. A phase equilibrium study in the system $KAlSi_3O_8$-$NaAlSi_3O_8$-SiO_2-Al_2SiO_5-H_2O and petrogenetic implications. *American Mineralogist*. 1994. Vol. 79. N 5-6, p. 504-512.

59. Yue Liao, Chunjing Wei, Rehman H.U. Titanium in calcium amphibole: Behavior and thermometry. *American Mineralogist*. 2021. Vol. 106. N 2, p. 180-191. DOI: 10.2138/am-2020-7409

60. Erdmann S., Rucheng Wang, Fangfang Huang et al. Titanite: A potential solidus barometer for granitic magma systems. *Comptes Rendus Géoscience*. 2019. Vol. 351. N 8, p. 551-561. DOI: 10.1016/j.crte.2019.09.002

61. Xiaoyan Li, Chao Zhang. Machine Learning Thermobarometry for Biotite-Bearing Magmas. *Journal of Geophysical Research*: *Solid Earth*. 2022. Vol. 127. Iss. 9. N e2022JB024137. DOI: 10.1029/2022JB024137

62. Xue-Ming Yang. Estimation of crystallization pressure of granite intrusions. *Lithos*. 2017. Vol. 286-287, p. 324-329. DOI: 10.1016/j.lithos.2017.06.018

63. Mills K.C., Karagadde S., Lee P.D. et al. Calculation of Physical Properties for Use in Models of Continuous Casting Process-Part 1: Mould Slags. *ISIJ International*. 2016. Vol. 56. Iss. 2, p. 264-273. DOI: 10.2355/isijinternational.ISIJINT-2015-364

64. Anderson J.L. Mineral Equilibria and Crystallization Conditions in the Late Precambrian Wolf River Rapakivi Massif, Wisconsin. *American Journal of Science*. 1980. Vol. 280. Iss. 4, p. 289-332. DOI: 10.2475/ajs.280.4.289

65. Eklund O., Shebanov A., Fröjdö S. et al. A flow-foliated ignimbrite related to the Åland rapakivi granite in SW Finland. *Terra Nova*. 1996. Vol. 8. Iss. 6, p. 548-557. DOI: 10.1111/j.1365-3121.1996.tb00784.x

66. Whitney D.L., Evans B.W. Abbreviations for names of rock-forming minerals. *American Mineralogist*. 2010. Vol. 95. N 1, p. 185-187. DOI: 10.2138/am.2010.3371

Authors: **Alexey V. Berezin,** *Candidate of Geological and Mineralogical Sciences, Senior Researcher* (*Institute of Precambrian Geology and Geochronology RAS, Saint Petersburg, Russia*), *https://orcid.org/0000-0002-5324-5840*, **Ilona V. Rogova,** *Postgraduate Student* (*Empress Catherine II Saint Petersburg Mining University, Saint Petersburg, Russia*), *i.l.o.n.a.borisova@yandex.ru*, *https://orcid.org/0009-0004-3547-3681*, **Sergey G. Skublov,** *Doctor of Geological and Mineralogical Sciences, Chief Researcher* (*Institute of Precambrian Geology and Geochronology RAS, Saint Petersburg, Russia*), *Professor* (*Empress Catherine II Saint Petersburg Mining University, Saint Petersburg, Russia*), *https://orcid.org/0000-0002-5227-4260*, **Evgeny I. Grokhotov,** *Executive Director of the Problem Oriented Laboratory* (*Empress Catherine II Saint Petersburg Mining University, Saint Petersburg, Russia*), *https://orcid.org/0000-0002-4620-2383*.

The authors declare no conflict of interests.

This is an open access article under the CC BY 4.0 license